Title
Sulfonamido tripods: Tuning redox potentials via ligand modifications

Authors
Lau, Nathanael
Ziller, Joseph W
Borovik, AS

Publication Date
2015

DOI
10.1016/j.poly.2014.09.014

Peer reviewed

Published in final edited form as:
Polyhedron. 2015 January 8; 85: 777–782. doi:10.1016/j.poly.2014.09.014.

Sulfonamido tripods: tuning redox potentials via ligand modifications

Nathanael Lau, **Joseph W. Ziller**, and **A.S. Borovik**
Department of Chemistry, University of California – Irvine, 1102 Natural Sciences II, Irvine, California 92697-2025, United States

Abstract

A series of Fe^{II}–OH_2 complexes were synthesized with ligands based on the tetradentate sulfonamido tripod *N*,*N*',*N*''-[2,2',2''-nitrilotris(ethane-2,1-diyl)]-tris-({R-Ph}-sulfonamido). These complexes differ by the substituent on the aryl rings and were fully characterized, including their molecular structures via X-ray diffraction methods. All the complexes were five-coordinate with trigonal bipyramidal geometry. A linear correlation was observed between the electronic effects of each ligand, given by the Hammett constants of the *para*-substituents, and the potential of the Fe^{II}/Fe^{III} redox couple, which were determined using cyclic voltammetry. It was found that the range of redox potentials for the complexes spanned approximately 160 mV.

1. Introduction

The structure and function of metal complexes can be understood within the context of the relationships between the primary and secondary coordination spheres.[1–3] These relationships are best illustrated in metalloproteins, in which the protein-induced microenvironments at the active site influence physical properties and reactivity. For instance, the electrochemical studies on a variety of metalloproteins showed that control of redox potentials can occur with modulations of either the primary or secondary coordination spheres. In series of studies, Lu showed that changes in the primary and secondary coordination spheres of a single Cu center had a large impact on the $Cu^{I/}Cu^{II}$ redox process in blue copper proteins.[4–6] Relatively small changes in redox potentials resulted when a tyrosine residue near the Fe^{III} center in rubredoxin was modified with nonnative tyrosine residues with differing *para*-substituents.[7] Analysis of electrochemical measurements did however demonstrate strong correlation between the reduction potential of the Fe^{III} center and the Hammett constants (σ_p) of the *para*-substituent of the nonnative tyrosine-based residues. Larger changes were reported in a series of mutated Fe superoxide dismutases, in which a single point mutation caused a change of greater than 500 mV for the $Fe^{II/}Fe^{III}$ redox couple.[8]

Correspondence to: A.S. Borovik.

Numerous synthetic systems have also shown that varying the structural features on ligands can control redox processes.[9–12] The recent work of Costas illustrates how physical properties of Fe complexes can be varied through modification of ring substituents of a coordinated pyridine ligand.[13] Moreover, intramolecular hydrogen bonds (H-bonds) within the secondary coordination sphere can alter the redox potential of transition metal complexes.[14–17] We have been investigating the effects on adjustments in both coordination spheres in synthetic systems through the rational design of multidentate ligands. Most of our work has examined the effects of the secondary coordination sphere, whereby control is achieved through intramolecular H-bonds.[3,18,19] More recently we have been exploring the chemistry associated with the tetradentate sulfonamide-based tripodal ligand *N*,*N*',*N*''-(nitrilotris(ethane-2,1-diyl))tris(2,4,6-trimethyl-benzenesulfonamido) ($[MST]^{3-}$). Mountford first introduced these types of tripodal ligands[20,21] and we have shown that $[MST]^{3-}$ can form hetero- and homobimetallic complexes containing intramolecular H-bonds.[19,22–24] In this report, we describe the preparation and chemistry for a series of monomeric $Fe^{II}–OH_2$ complexes (Fig. 1, Scheme 1) with different sulfonamido tripodal ligand $[RST]^{3-}$, (*N*,*N*',*N*''-[2,2',2''-nitrilotris(ethane-2,1-diyl)]-tris-({R-Ph}-sulfonamido) R = OMe, Me, H, Cl, CF_3). The ligands differ by the *para*-substituent of the aryl group on the sulfonamido arms and allowed us to examine how these modifications correlated with individual properties of the $Fe^{II}–OH_2$ complexes. Our findings illustrated that the electrochemical properties of the complexes can be predictably tuned through modulation of the ligand but other physical properties are not significantly affected by these modifications.

2. Experimental

2.1 General methods

All reagents were purchased from commercial sources and used as received unless otherwise noted. Solvents were sparged with argon and dried over columns containing Q-5 and molecular sieves. The syntheses of the ligands were carried out in air and the preparations of metal complexes were conducted in a Vacuum Atmospheres, Co. drybox under nitrogen or argon atmosphere. Sodium hydride (NaH) as a 60% dispersion in mineral oil was filtered with a medium porosity glass-fritted funnel and washed 5 times each with pentane and Et_2O. Solid NaH was dried under vacuum and stored under inert atmosphere. $Fe(OAc)_2$ was prepared by literature procedures.[25] Water was degassed by five freeze-pump-thaw cycles and stored under inert atmosphere. The tripodal ligands H_3MOST, H_3TST, and H_3PST were synthesized following literature procedures with modifications–see supporting information for details.[26–28]

2.2 Preparation of Ligands

2.2.1 N,N',N''-(nitrilotris(ethane-2,1-diyl))tris(4-(trifluoromethyl)-benzene-sulfonamide) (H_3F_3ST)—To a 250 mL round bottom flask containing tris(2-aminoethyl)amine (tren) (0.25 g, 1.7 mmol) and NaOH (0.33 g, 8.2 mmol) in water (20 mL), 4-(trifluoromethyl)benzenesulfonyl chloride (1.3 g, 5.4 mmol) dissolved in Et_2O (10 mL) was added dropwise at room temperature with vigorous stirring. After allowing the reaction mixture to stir for 2 days, the Et_2O was removed under reduced pressure and the resulting white precipitate was collected on a medium porosity glass-fritted funnel and washed with

water. The resulting white power was dried under reduced pressure overnight, then dissolved in dichloromethane (CH_2Cl_2) (100 mL) and dried with anhydrous sodium sulfate. After filtering off the insoluble species, the solvent was removed and the residue was dried under vacuum at 45 °C for 5 h. The residue was brought into the dry box, redissolved in CH_2Cl_2 (10 mL), and precipitated with pentane to give 0.81 g (62%) of an ivory powder. FTIR (KBr disc, cm^{-1}, selected bands): 3353, 3303, 3262, 3106, 2965, 2824, 1610, 1405, 1323, 1165, 1106, 1062, 958, 846, 713, 602, 554. ^{1}H NMR (500 MHz, $CDCl_3$, ppm): 2.61 (t, 2H), 3.06 (t, 2H), 5.91 (br s, 1H NH), 7.79 (d, 2H), 8.08 (d, 2H). ^{13}C NMR (500 MHz, $CDCl_3$, ppm): 41.5, 54.8, 126.8, 128.0, 129.3, 143.6. HRMS (ES+, m/z): Exact mass calcd for $C_{27}H_{27}N_4O_6S_3F_9$: 771.10, Found: 771.04.

2.2.2 N,N',N''-(nitrilotris(ethane-2,1-diyl))tris(4-chloro-benzenesulfonamide) (H_3CST)—Prepared in an analogous manner to H_3F_3ST using tren (0.26 g, 1.8 mmol), NaOH (0.34 g, 8.4 mmol), 4-chlorobenzenesulfonyl chloride (1.2 g, 5.6 mmol) to give 0.66 g (55%) product. FTIR (KBr disc, cm^{-1}, selected bands): 3291, 3093, 2957, 2850, 1587, 1477, 1396, 1327, 1162, 1094, 955, 825, 753, 618, 567. ^{1}H NMR (500 MHz, $CDCl_3$, ppm): 2.55 (t, 2H), 2.98 (t, 2H), 5.91 (br s, 1H NH), 7.49 (d, 2H), 7.86 (d, 2H). ^{13}C NMR (500 MHz, $CDCl_3$, ppm): 41.4, 54.7, 129.0, 129.9, 138.5, 139.6. HRMS (ES+, m/z): Exact mass calcd for $C_{24}H_{27}N_4O_6S_3Cl_3$: 669.02, Found: 669.01.

2.3 Preparation of the complexes

2.3.1 [NMe_4][$Fe^{II}F_3$ST(OH_2)]—A solution of H_3F_3ST (300 mg, 0.39 mmol) dissolved in 6 mL of anhydrous dimethylacetamide (DMA) was treated with solid NaH (28 mg, 1.2 mmol). The mixture was stirred until gas evolution ceased. $Fe(OAc)_2$ (68 mg, 0.39 mmol) and NMe_4OAc (52 mg, 0.39 mmol), were added to the cloudy white reaction, and the solution was stirred. After 3 h, 5 mL of Et_2O was added to the yellow solution to aid the precipitation of NaOAc. The reaction mixture was filtered through a medium porosity glass-fritted funnel to remove the insoluble species and the filtrate was dried under vacuum. The resulting pale yellow solid was redissolved in 5 mL of acetonitrile (MeCN), stirred for 20 min, and filtered using a fine porosity glass-fritted funnel. The filtrate was concentrated under vacuum to *ca*. 1 mL and treated with Et_2O (10 mL) then pentane (40 mL) to precipitate a pale yellow solid. The pale yellow solid was collected on a medium porosity glass-fritted funnel and dried under vacuum to give 182 mg (91%) of product. FTIR (KBr disc, cm^{-1}, selected bands): 3413, 3046, 2964, 2902, 2861, 1608, 1490, 1403, 1326, 1263, 1134, 1062, 976, 821, 710, 622, 605. MS (ES−, m/z): Exact mass calcd for $C_{27}H_{24}N_4O_6S_3F_9Fe$: 823.0, Found: 823.1. This salt, presumably [NMe_4][$Fe^{II}F_3$ST] (103 mg, 0.12 mmol) in 5 mL of CH_2Cl_2, was treated with H_2O (8 μL, 0.46 mmol) in one portion *via* a syringe and the mixture was stirred. After 15 min, volatiles were removed under reduced pressure and the solid residue was redissolved in CH_2Cl_2 (6 mL), filtered through a medium porosity glass-fritted funnel, and layered under pentane. White needle crystals were collected via filtration and dried under vacuum, to give 98 mg (94%) of crystalline product. Elemental analysis calcd for [NMe_4][$Fe^{II}F_3$ST(OH_2)] $C_{31}H_{38}N_5O_7S_3F_9Fe$: C, 40.66; H, 4.18; N, 7.65%, Found: C, 40.74; H, 4.06; N, 7.32%. FTIR (KBr disc, cm^{-1}, selected bands): 3340, 3044, 2964, 2899, 2860, 1608, 1490, 1403, 1327, 1261, 1136, 1062, 977, 825,

710, 622, 605. (Nujol, cm^{-1}): 3295 (OH). μ_{eff} (μ_B): 4.7(2). $E_{1/2}$ (MeCN): −0.284 V vs. $[FeCp_2]^{0/+}$.

2.3.2 $[NMe_4][Fe^{II}CST(OH_2)]$—This salt was prepared in an analogous manner to $[NMe_4][Fe^{II}F_3ST(OH_2)]$ using H_3CST (180 mg, 0.27 mmol), NaH (20 mg, 0.81 mmol), $Fe(OAc)_2$ (47 mg, 0.27 mmol), NMe_4OAc (38 mg, 0.28 mmol) to isolate a pale yellow powder, which presumably was the $[NMe_4][Fe^{II}CST]$ salt (141 mg, 66%). FTIR (KBr disc, cm^{-1}, selected bands): 3341, 3036, 2960, 2898, 2856, 1636, 1581, 1477, 1392, 1251, 1141, 1084, 975, 823, 751, 630, 593. MS (ES−, m/z): Exact mass calcd for $C_{24}H_{24}N_4O_6S_3Cl_3Fe$: 720.9, Found: 721.0. The isolated $[NMe_4][Fe^{II}CST]$ (33 mg, 0.04 mmol) was treated with H_2O (3 μL, 0.17 mmol) in an analogous manner to $[NMe_4][Fe^{II}F_3ST(OH_2)]$ to give 28 mg (83%) of crystalline product. Elemental analysis calcd for $[NMe_4][Fe^{II}CST(OH_2)]$ $C_{28}H_{38}N_5O_7S_3Cl_3Fe$: C, 41.26; H, 4.70; N, 8.59%, Found: C, 41.09; H, 4.57; N, 8.22%. FTIR (KBr disc, cm^{-1}, selected bands): 3313, 3036, 2964, 2899, 2855, 1580, 1476, 1391, 1247, 1138, 1083, 975, 821, 751, 629, 593. (Nujol, cm^{-1}): 3303 (OH). μ_{eff} ($CDCl_3$, μ_B): 4.8(3). $E_{1/2}$ (MeCN): −0.338 V vs. $[FeCp_2]^{0/+}$.

2.3.3 $[NMe_4][Fe^{II}PST(OH_2)]$—This salt was prepared in an analogous manner to $[NMe_4][Fe^{II}F_3ST(OH_2)]$ using H_3PST (300 mg, 0.53 mmol), NaH (38 mg, 1.6 mmol), $Fe(OAc)_2$ (92 mg, 0.53 mmol), NMe_4OAc (71 mg, 0.53 mmol) to isolate a pale yellow powder, which presumably was the $[NMe_4][Fe^{II}PST]$ salt (340 mg, 93%). FTIR (KBr disc, cm^{-1}, selected bands): 3297, 3035, 2955, 2897, 2853, 1489, 1445, 1246, 1132, 974, 821, 761, 715, 694, 608, 586. MS (ES−, m/z): Exact mass calcd for $C_{24}H_{27}N_4O_6S_3Fe$: 619.0, Found: 619.1. The isolated $[NMe_4][Fe^{II}PST]$ salt (26 mg, 0.04 mmol) was treated with H_2O (3 μL, 0.14 mmol) in an analogous manner to $[NMe_4][Fe^{II}F_3ST(OH_2)]$ to give 27 mg (85%) of crystalline product. Elemental analysis calcd for $[NMe_4][Fe^{II}PST(OH_2)]$ $C_{28}H_{41}N_5O_7S_3Fe$: C, 47.25; H, 5.81; N, 9.84%, Found: C, 47.19; H, 5.53; N, 9.63%. FTIR (KBr disc, cm^{-1}, selected bands): 3313, 3034, 2957, 2897, 2854, 1489, 1445, 1247, 1132, 975, 821, 761, 714, 694, 608, 586. (Nujol, cm^{-1}): 3290 (OH). μ_{eff} ($CDCl_3$, μ_B): 4.9(9). $E_{1/2}$ (MeCN): −0.394 V vs. $[FeCp_2]^{0/+}$.

2.3.4 $[NMe_4][Fe^{II}TST(OH_2)]$—This salt was prepared in an analogous manner to $[NMe_4][Fe^{II}F_3ST(OH_2)]$ using H_3TST (300 mg, 0.49 mmol), NaH (30 mg, 1.2 mmol), $Fe(OAc)_2$ (71 mg, 0.41 mmol), NMe_4OAc (55 mg, 0.41 mmol) to isolate a pale yellow powder which presumably was the $[NMe_4][Fe^{II}TST]$ salt (310 mg, 86%). FTIR (KBr disc, cm^{-1}, selected bands): 3264, 3037, 2958, 2896, 2850, 1599, 1492, 1325, 1246, 1138, 975, 818, 664, 600, 555. MS (ES−, m/z): Exact mass calcd for $C_{27}H_{33}N_4O_6S_3Fe$: 661.1, Found: 661.2. The isolated solid $[NMe_4][Fe^{II}TST]$ salt (56 mg, 0.08 mmol) was treated with H_2O (5 μL, 0.30 mmol) in an analogous manner to $[NMe_4][Fe^{II}F_3ST(OH_2)]$ to give 42 mg (74%) of crystalline product. Elemental analysis calcd for $[NMe_4][Fe^{II}TST(OH_2)]$ $C_{31}H_{47}N_5O_7S_3Fe$: C, 49.40; H, 6.28; N, 9.29%, Found: C, 49.21; H, 6.04; N, 9.02%. FTIR (KBr disc, cm^{-1}, selected bands): 3281, 3036, 2957, 2896, 2852, 1599, 1491, 1244, 1138, 975, 817, 664, 599, 554. (Nujol, cm^{-1}): 3249 (OH). μ_{eff} ($CDCl_3$, μ_B): 4.8(1). $E_{1/2}$ (MeCN): −0.419 V vs. $[FeCp_2]^{0/+}$.

2.3.5 [NMe_4][$Fe^{II}MOST(OH_2)$]—This salt was prepared in an analogous manner to [NMe_4][$Fe^{II}F_3ST(OH_2)$] using H_3MOST (200 mg, 0.30 mmol), NaH (22 mg, 0.91 mmol), $Fe(OAc)_2$ (53 mg, 0.30 mmol), NMe_4OAc (41 mg, 0.30 mmol) to isolate a pale yellow powder ([NMe_4][Fe^{II}MOST]) in 76% yield. FTIR (KBr disc, cm^{-1}, selected bands): 3264, 3036, 2958, 2898, 2847, 1597, 1496, 1304, 1250, 1134, 1013, 975, 818, 667, 601, 564. MS (ES−, m/z): Exact mass calcd for $C_{27}H_{33}N_4O_9S_3Fe$ 709.1, Found 709.1. The isolated solid [NMe_4][Fe^{II}MOST] (62 mg, 0.08 mmol) was treated with H_2O (6 μL, 0.31 mmol) in an analogous manner to [NMe_4][Fe^{II} $F_3ST(OH_2)$] to give 61 mg (96%) of crystalline product. Elemental analysis calcd for [NMe_4][$Fe^{II}MOST(OH_2)$] $C_{31}H_{47}N_5O_{10}S_3Fe$: C, 46.44; H, 5.91; N, 8.73%, Found: C, 46.34; H, 5.62; N, 8.66%. FTIR (KBr disc, cm^{-1}, selected bands): 3302, 3039, 2961, 2897, 2843, 1597, 1496, 1306, 1254, 1134, 1025, 972, 832, 667, 603, 564. (Nujol, cm^{-1}): 3247 (OH). μ_{eff} ($CDCl_3$, μ_B): 4.9(3). $E_{1/2}$ (MeCN): −0.441 V vs. $[FeCp_2]^{0/+}$.

2.4 Physical Methods

Elemental analyses were performed on a Perkin-Elmer 2400 CHNS analyzer. ^{1}H NMR and ^{13}C NMR were recorded on a Bruker DRX500 spectrometer. Fourier transform infrared (FTIR) spectra were collected on a Varian 800 Scimitar Series FTIR spectrometer. High-resolution mass spectra were collected using Waters Micromass LCT Premier Mass Spectrometer. Perpendicular-mode X-band electron paramagnetic resonance (EPR) spectra were collected using a Bruker EMX spectrometer at 77K using liquid nitrogen. Solution effective magnetic moments were measured by the Evans' method on a Bruker DRX500 spectrometer using flame sealed standard cores of 1:1 $CHCl_3$:$CDCl_3$.[29] Cyclic voltammetric experiments were conducted using a CH1600C electrochemical analyzer. A 2.0 mm glassy carbon electrode was used as the working electrode at scan velocities 0.1 Vs^{-1} unless otherwise noted. A cobaltocenium/cobaltocene couple ($[CoCp_2]^{0/+}$) was used as an internal reference then scaled against the ferrocene/ferrocenium couple ($[Fe\ Cp_2]^{0/+}$).[30] Tetrabutylammonium hexafluorophosphate (TBAP) was use as the supporting electrolyte at a concentration of 0.1 M. Electrochemical values are reported as the average of three independent measurements.

2.5 Crystallography

A Bruker SMART APEX II diffractometer and the APEX2 program package was used to determine the unit-cell parameters and for data collection. Crystallographic details are summarized in the supporting information and in Table S1.

3. Results and discussion

3.1. Preparation and Properties of the [NMe_4][$Fe^{II}RST(OH_2)$]

The five salts were prepared using the synthetic route described in Scheme 1. The starting H_3RST compounds were deprotonated with 3 equivalents of NaH in DMA. Metallation with $Fe(OAc)_2$ and metathesis with NMe_4OAc resulted in the formation of Fe^{II} complexes as the $[NMe_4]^+$ salt. Adding Et_2O facilitated precipitation of NaOAc from DMA that was removed from the reaction mixture *via* filtration. The Fe salts were isolated and their properties are consistent with a formulation of [NMe_4][Fe^{II}RST]. However, we were never able to obtain

acceptable elemental analysis for any of these salts, possibly because a small amount of the complexes were five-coordinate, which could arise from a weakly interacting solvent molecules.

To prepare the Fe^{II}–OH_2 complexes, CH_2Cl_2 solutions of each $[Fe^{II}RST]^-$ complex were treated with four equivalents of water and the mixtures were allowed to stir for 5 minutes. Volatiles were removed under reduced pressure, and the resulting salts were recrystallized from solutions in CH_2Cl_2 that were layered under pentane to afford crystalline products in yields ranging from 74–96%.

The $[NMe_4][Fe^{II}RST(OH_2)]$ salts were characterized by EPR and FTIR spectroscopies, solution effective magnetic moment measurements, and elemental analysis. The perpendicular-mode EPR spectra measured at 77 K did not contain any features, which is consistent with each complex having a high spin Fe^{II} center. This premise is supported by the room temperature solution effective magnetic moment of the complexes determined using the Evans' method. The effective magnetic moments for the complexes were statistically the same and matched closely with the spin-only magnetic moment value of 4.9 μ_B. These values can be attributed to an S=2 spin ground state from the five-coordinate Fe^{II} complexes. FTIR spectra of the complexes recorded as a Nujol mull revealed the presence of peaks that ranged between 3300 to 3250 cm^{-1}, which is consistent with O–H vibrations from a coordinated water molecule.

3.2 Solid-State Molecular Structures of $[Fe^{II}RST(OH_2)]^-$ Complexes

The molecular structures of the $[NMe_4][Fe^{II}RST(OH_2)]$ salts were characterized by X-ray diffraction methods. Selected bond lengths and bond angles are given in Table 1 and representative thermal ellipsoid diagrams of $[Fe^{II}TST(OH_2)]^-$ and $[Fe^{II}PST(OH_2)]^-$ are shown in Figure 2. All of the salts crystallized with their anionic complexes as monomers, with one distinct metal complex per asymmetric unit cell for three of the five salts: $[NMe_4][Fe^{II}CST(OH_2)]$, $[NMe_4][Fe^{II}PST(OH_2)]$, and $[NMe_4][Fe^{II}TST(OH_2)]$. Two crystallographically distinct but chemically equivalent complexes were contained per asymmetric unit cell in $[NMe_4][Fe^{II}F_3ST(OH_2)]$ and $[NMe_4][Fe^{II}MOST(OH_2)]$.

The $[Fe^{II}RST(OH_2)]^-$ complexes had similar N_4O primary coordination sphere around the Fe^{II} center, whereby the trigonal plane is defined by the three deprotonated nitrogen atoms (N2, N3, N4) from the sulfonamido groups. One apical position (N1) is occupied by the amine nitrogen atom of the $[RST]^{3-}$ ligands and the other site is taken by oxygen atom (O1) from the external aqua ligand. The Fe^{II} center is displaced from the trigonal plane in each complex (~ 0.35 Å) toward the O1. Each complex shows a modest distortion from trigonal bipyramidal (tbp) coordination geometry, as gauged using the structural parameter τ: the values for the complexes range from 0.826 – 0.859.[31] The distortions from idealized tbp could be caused, in part, from a Jahn-Teller effect that should be present in high-spin d^6 metal complex having local C_3 symmetry.[32] This effect should be small because it arises from the d_{xz} and d_{yz} orbitals that are formally non-bonding. A larger contributor to the distortion is the contraction of the N1–Fe1–O1 angle, which in each complex is less than 175°. Note that the "bend" in the angle is such that O1 is positioned towards two of the sulfonamido arms containing O2 and O4, with O1···O2 distances ranging from 2.672 –

2.763 Å and the O1···O4 distances ranging from 2.676 – 2.782 Å. Both these distances are indicative of H-bonds formed between the aqua ligand and oxygen atoms of the sulfonamido groups from two different arms of the $[RST]^{3-}$ ligands. These two intramolecular H-bonds undoubtedly assist in positioning the aqua ligand within the complexes.[33] The other metrical parameters are consistent with values found in similar Fe^{II} complexes.[34]

3.3 Effects of the Substituents on the $[RST]^{3-}$ Ligands: Vibrational Properties

The *para*-substituents on aryl groups of the $[RST]^{3-}$ ligands varied in their electronic effects, which often causes predictable changes in the physical and chemical properties within compounds. However, we did not observe any correlations between the substituents and either the vibrational properties of the coordinated aqua ligands or the structural parameters of the complexes. The energies of the ν(OH) bands would be expected to trend based on the electronic effects that the substituents have on the electron-withdrawing ability of the tripodal ligands. As the electron density at the metal center decreases because of the changes in the ligand field provided by the different $[RST]^{3-}$ ligands, the acidity of the aqua ligand should also increase, which would be reflected in an decrease in the energy of the ν(OH) band. Yet this analysis is complicated by the presence of intramolecular H-bonds involving the coordinated aqua ligand. The electronic effects of the substituents on the $[RST]^{3-}$ also affects the ability of these ligands to act as H-bond acceptors, with the more electron-withdrawing ligands (e.g., R = $–CF_3$) being the poorest at accepting a H-bond. Therefore, the effects of increased acidity of the Fe–OH unit versus the decrease in H-bond accepting within the series of $[Fe^{II}RST(OH_2)]^-$ complexes could be nearly offsetting and result in the observed lack of a correlative property.

3.4. Effects of the Substituents on the $[RST]^{3-}$ Ligands: Structural Properties

There are no statistically significant trends between the electronic properties of the *para*-substituent on the $[RST]^{3-}$ ligand and the structural parameters of the $[Fe^{II}RST(OH_2)]^-$ complexes. For example, the Fe1–O1 bond distances should change in accordance with the effects of the substituent on the $[RST]^{3-}$ ligand, with shortest bond distance predicted to be found in $[Fe^{II}F_3ST(OH_2)]^-$. However, $[Fe^{II}TST(OH_2)]^-$ and $[Fe^{II}CST(OH_2)]^-$ had statistically equivalent Fe1–O1 bond lengths and were the shortest values in the series. In addition, the average Fe1–N_{eq} bond distances in $[Fe^{II}TST(OH_2)]^-$, $[Fe^{II}PST(OH_2)]^-$, $[Fe^{II}CST(OH_2)]^-$, $[Fe^{II}F_3ST(OH_2)]^-$ are statistically the same.

3.5. Effects of the Substituents on the $[RST]^{3-}$ Ligands: Redox Properties

The electrochemical properties of the $[Fe^{II}RST(OH_2)]^-$ complexes were explored using cyclic voltammetry (Fig. 3). A quasi-reversible one-electron process was observed for each complex, which was assigned as the Fe^{II}/Fe^{III} couple. In contrast to the discussion above, the redox potentials for this couple was dependent on the electronic effects of the ligand, as shown by a linear Hammett plot of the $E_{1/2}$ of the Fe^{II}/Fe^{III} couple vs. the σ_p of the ligand *para*- substituents (Fig. 4).[35] The high r^2 value of 0.99 for the linear best-fit demonstrates a high correlation between the oxidation potentials and the electronic properties the different $[RST]^{3-}$ ligands. Complexes with ligands that contained *para*-substituents with greater

electron-withdrawing ability shifted the Fe^{II}/Fe^{III} couple to more positive potentials, which is consistent with these ligands stabilizing the $Fe^{II}–OH_2$ complexes.[36]

The potential difference between the complex with the most electron-withdrawing ligand, $[F_3ST]^{3-}$, and the most electron-donating ligand, $[MOST]^{3-}$, was 157 mV or a free energy difference of 3.62 kcal mol^{-1}. This corresponds to an approximately 450-fold decrease in the rate of electron transfer between the complex with $[F_3ST]^{3-}$ and $[MOST]^{3-}$ at room temperature. Moreover, the slope of the linear trend line is 4.5 kcal mol^{-1} per Hammett unit. This is greater than the slope of the linear trend line of 0.7 kcal mol^{-1} per Hammett unit observed in a study on synthetic rubredoxins that examined only secondary coordination sphere effects,[7] but less than the slope of the linear trend line of 9.9 kcal mol^{-1} per Hammett unit observed in a study on a series of Fe^{II} bis-terpyridyl complexes that examined primary coordination sphere effects.[11]

5. Summary and conclusions

The present study describes the synthesis and characterization of a series of $Fe^{II}–OH_2$ complexes with sulfonamido tripodal ligands. These ligands were designed to vary the properties at the iron center via modifying the *para*-substituent of the aryl group on the ligand sulfonamido arms. The $[Fe^{II}RST(OH_2)]^-$ complexes have many similar properties despite the modulation of the ligands. Structurally, all of the complexes in this series have nearly the same distorted tbp geometry with small metrical differences in their primary coordination spheres. The complexes were determined to have high spin S=2 Fe^{II} centers, as each of their effective magnetic moments agreed closely with the spin-only magnetic moment value of 4.9 μ_B. Moreover, the vibrational properties of the $[Fe^{II}RST(OH_2)]^-$ complexes, specifically the energies of the bands associated with the ν(OH), did not show a correlation with the substituent effects on the $[RST]^{3-}$ ligands. We attribute the lack of correlative relationships to the presence of intramolecular H-bonds within each complex. Comparing the H-bond donating properties of the $Fe–OH_2$ unit with the H-bond accepting ability of the $[RST]^{3-}$ ligands throughout the series of complexes led us to suggest that the H-bonds mitigate the influence that the substituents may have on these properties of the complexes. Nevertheless, we observed a small, but significant trend in the redox potentials within the series of $[Fe^{II}RST(OH_2)]^-$ complexes. A linear trend between the redox potentials of the Fe^{II}/Fe^{III} couples and the σ_p for the ligand *para*-substituent was demonstrated, illustrating that the electrochemical properties of the complexes can be tuned by modifying the $[RST]^{3-}$ ligands.

Supplementary Material

Refer to Web version on PubMed Central for supplementary material.

Acknowledgments

The authors thank the National Institutes of Health, USA (GM050781).

Appendix A. Supplementary Data

CCDC 982221 for $[NMe_4][Fe^{II}F_3ST(OH_2)]$; 982222 for $[NMe_4][Fe^{II}CST(OH_2)]$; 982223 for $[NMe_4][Fe^{II}PST(OH_2)]$; 982224 for $[NMe_4][Fe^{II}TST(OH_2)]$; 982225 for $[NMe_4][Fe^{II}MOST(OH_2)]$; these files contains the supplementary crystallographic data for the salt as indicated. These data can be obtained free of charge via http://www.ccdc.cam.ac.uk/conts/retrieving.html, or from the Cambridge Crystallographic Data Centre, 12 Union Road, Cambridge CB2 1EZ, UK; fax: (+44) 1223-336-033; or deposit@ccdc.cam.ac.uk. Supplementary data associated with this article can be found, in the online version.

References

1. Colquhoun HM, Stoddart JF, Williams DJ. Angew. Chem., Int. Ed. Engl. 1986; 25:487–507.
2. Borovik AS. Acc. Chem. Res. 2005; 38:54–61. [PubMed: 15654737]
3. Shook RL, Borovik AS. Inorg. Chem. 2010; 49:3646–3660. [PubMed: 20380466]
4. Garner DK, Vaughan MD, Hwang HJ, Savelieff MG, Berry SM, Honek JF, Lu Y. J. Am. Chem. Soc. 2006; 128:15608–15617. [PubMed: 17147368]
5. Marshall NM, Garner DK, Wilson TD, Gao Y-G, Robinson H, Nilges MJ, Lu Y. Nature. 2009; 462:113–116. [PubMed: 19890331]
6. Farver O, Marshall NM, Wherland S, Lu Y, Pecht I. Proc. Natl. Acad. Sci. U. S. A. 2013; 110:10536–10540. [PubMed: 23759745]
7. Low DW, Hill MG. J. Am. Chem. Soc. 1998; 120:11536–11537.
8. Yikilmaz E, Rodgers DW, Miller A-F. Biochemistry. 2006; 45:1151–1161. [PubMed: 16430211]
9. Hong S, Hill LMR, Gupta AK, Naab BD, Gilroy JB, Hicks RG, Cramer CJ, Tolman WB. Inorg. Chem. 2009; 48:4514–4523. [PubMed: 19425614]
10. Sjödin M, Gätjens J, Tabares LC, Thuéry P, Pecoraro VL, Un S. Inorg. Chem. 2008; 47:2897–2908. [PubMed: 18271528]
11. Chambers J, Eaves B, Parker D, Claxton R, Ray PS, Slattery SJ. Inorg. Chim. Acta. 2006; 359:2400–2406.
12. Buttafava A, Fabbrizzi L, Perotti A, Poggi A, Poli G, Seghi B. Inorg. Chem. 1986; 25:1456–1461.
13. Prat I, Company A, Corona T, Parella T, Ribas X, Costas M. Inorg. Chem. 2013; 52:9229–9244. [PubMed: 23901826]
14. Mukherjee J, Lucas RL, Zart MK, Powell DR, Day VW, Borovik AS. Inorg. Chem. 2008; 47:5780–5786. [PubMed: 18498155]
15. Mareque Rivas JC, Hinchley SL, Metteau L, Parsons S. Dalton Trans. 2006:2316–2322. [PubMed: 16688319]
16. Tani F, Matsu-ura M, Nakayama S, Ichimura M, Nakamura N, Naruta Y. J. Am. Chem. Soc. 2001; 123:1133–1142. [PubMed: 11456666]
17. Suzuki N, Higuchi T, Urano Y, Kikuchi K, Uekusa H, Ohashi Y, Uchida T, Kitagawa T, Nagano T. J. Am. Chem. Soc. 1999; 121:11571–11572.
18. Hammes BS, Young VG Jr, Borovik AS. Angew. Chemie Int. Ed. 1999; 38:666–669.
19. Park YJ, Ziller JW, Borovik S. J. Am. Chem. Soc. 2011; 133:9258–9261. [PubMed: 21595481]
20. Schwarz AD, Chu Z, Mountford P. Organometallics. 2010; 29:1246–1260.
21. Schwarz AD, Herbert KR, Paniagua C, Mountford P. Organometallics. 2010; 29:4171–4188.
22. Lacy DC, Park YJ, Ziller JW, Yano J, Borovik AS. J. Am. Chem. Soc. 2012; 134:17526–17535. [PubMed: 22998407]
23. Park YJ, Cook SA, Sickerman NS, Sano Y, Ziller JW, Borovik AS. Chem. Sci. 2013; 4:717–726. [PubMed: 24058726]
24. Sano Y, Weitz AC, Ziller JW, Hendrich MP, Borovik AS. Inorg. Chem. 2013; 52:10229–10231. [PubMed: 23992041]

25. Weber B, Betz R, Bauer W, Schlamp S. Zeitschrift für Anorg. und Allg. Chemie. 2011; 637:102–107.
26. Warr RJ, Westra AN, Bell KJ, Chartres J, Ellis R, Tong C, Simmance TG, Gadzhieva A, Blake AJ, Tasker PA, Schröder M. Chem. - A Eur. J. 2009; 15:4836–4850.
27. Chen D, Motekaitis RJ, Murase I, Martell AE. Tetrahedron. 1995; 51:77–88.
28. Boon JM, Lambert TN, Smith BD, Beatty AM, Ugrinova V, Brown SN. J. Org. Chem. 2002; 67:2168–2174. [PubMed: 11925224]
29. Evans DF. J. Chem. Soc. 1959:2003–2005.
30. Connelly NG, Geiger WE. Chem. Rev. 1996; 96:877–910. [PubMed: 11848774]
31. Addison AW, Rao TN, Reedijk J, van Rijn J, Verschoor GC. J. Chem. Soc. Dalton Trans. 1984:1349.
32. Sickerman NS, Park YJ, Ng GK-Y, Bates JE, Hilkert M, Ziller JW, Furche F, Borovik AS. Dalton Trans. 2012; 41:4358–4364. [PubMed: 22334366]
33. Emsley J. Chem. Soc. Rev. 1980; 9:91.
34. Matson EM, Bertke JA, Fout AR. Inorg. Chem. 2014; 53:4450–4458. [PubMed: 24758308]
35. Leffler, JE.; Grunwald, E. Rates and Equilibria of Organic Reactions as Treated by Statistical, Thermodynamic, and Extrathermodynamic Methods. New York: Dover Publications; 1989. Reprint.
36. Tustin GJ, Lafitte VGH, Banks CE, Jones TGJ, Smith RB, Davis J, Lawrence NS. J. Organomet. Chem. 2007; 692:5173–5182.

Five new Fe(II)–OH_2 complexes with different sulfonamido tripodal ligands have been prepared and characterized. The complexes have different substituents on the aryl rings of each sulfonamide. Only a correlation between the properties of substituents and the redox potentials of the complexes were found that span 160 mV.

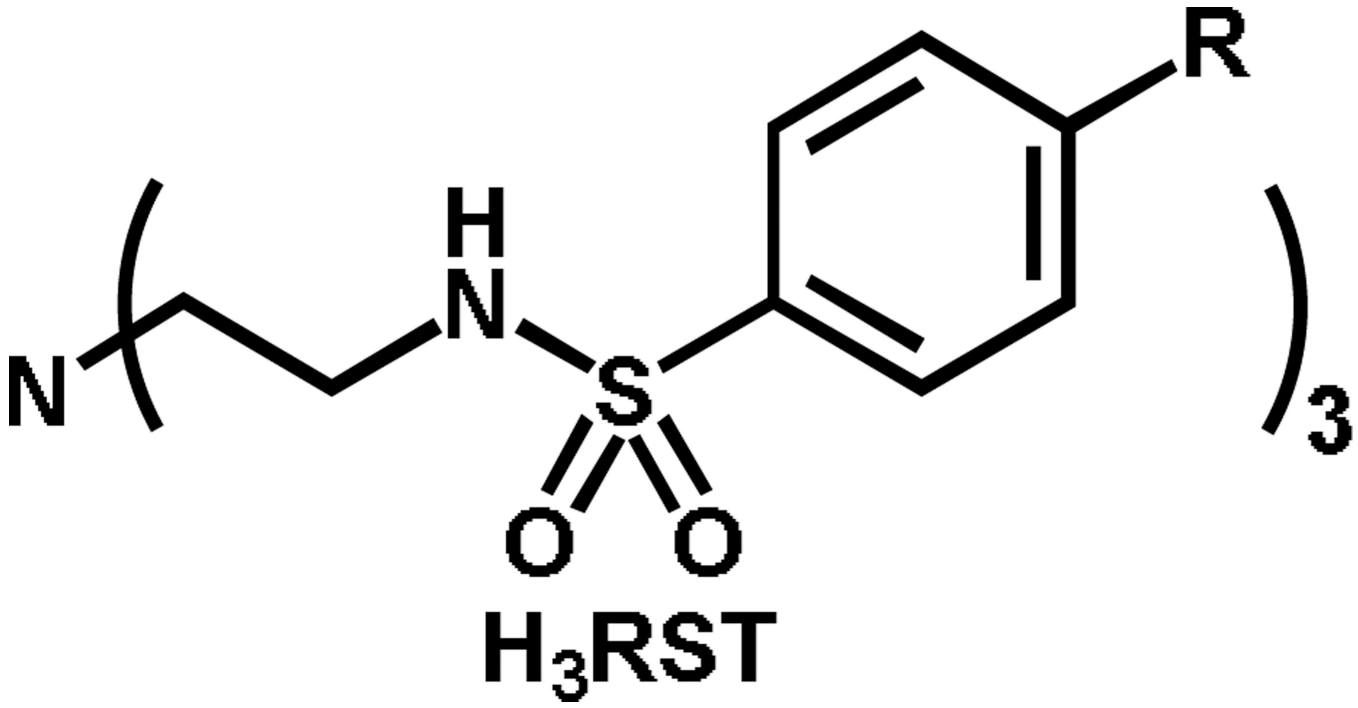

Fig. 1.

H_3RST compounds where R = $–CF_3$ ([H_3F_3ST]), –Cl ([H_3CST]), –H ([H_3PST]), $–CH_3$ ([H_3TST]), $–OCH_3$ ([H_3MOST]).

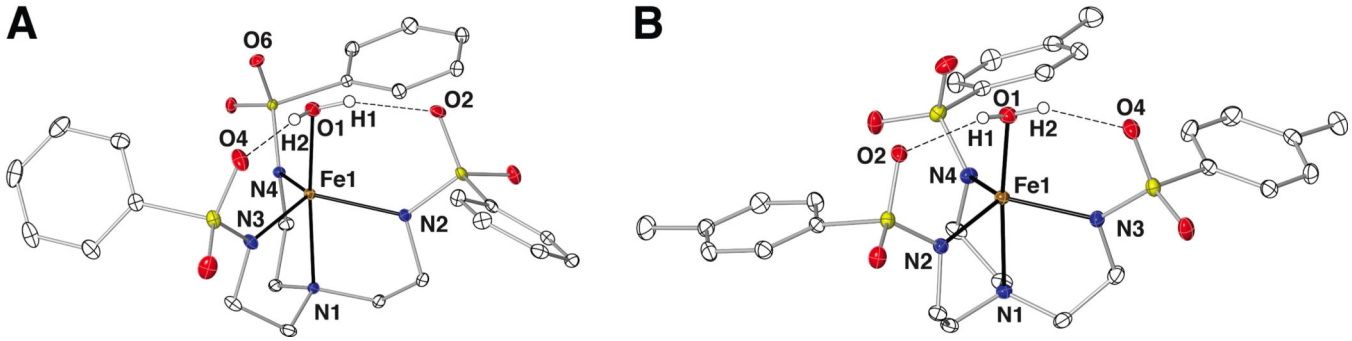

Fig. 2.

Thermal ellipsoid diagram depicting the molecular structure of (A) $[Fe^{II}PST(OH_2)]^-$ and (B) $[Fe^{II}TST(OH_2)]^-$. Ellipsoids are drawn at the 50% probability level, and only the aqua **H** atoms are shown for clarity.

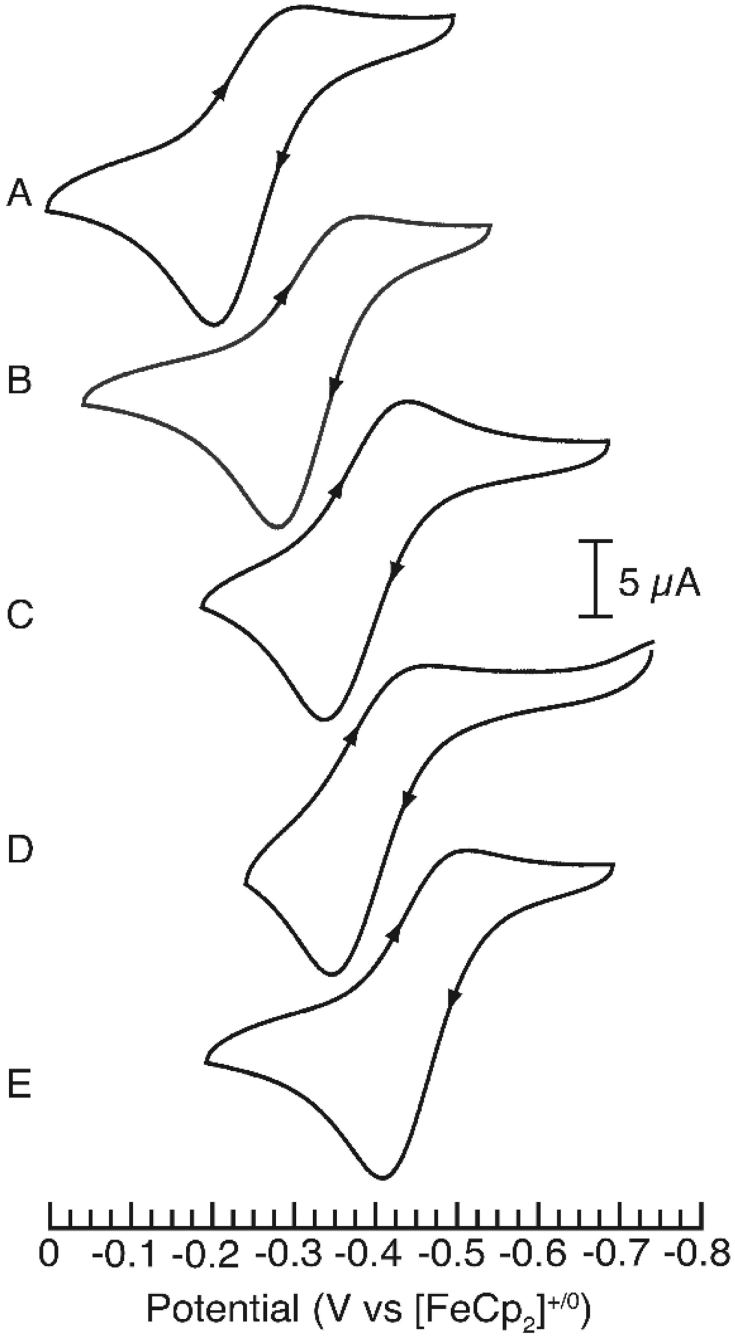

Fig. 3.

Cyclic voltammagram of (A) $[NMe_4][Fe^{II}F_3ST(OH_2)]$, (B) $[NMe_4][Fe^{II}CST(OH_2)]$, (C) $[NMe_4][Fe^{II}PST(OH_2)]$, (D) $[NMe_4][Fe^{II}TST(OH_2)]$, (E) $[NMe_4][Fe^{II}MOST(OH_2)]$ measured in MeCN (0.1 M TBAP). All voltammagrams were collected at 100 mV s^{-1} and internally referenced against $[CoCp_2]^{0/+}$, then scaled against $[FeCp_2]^{+/0}$.

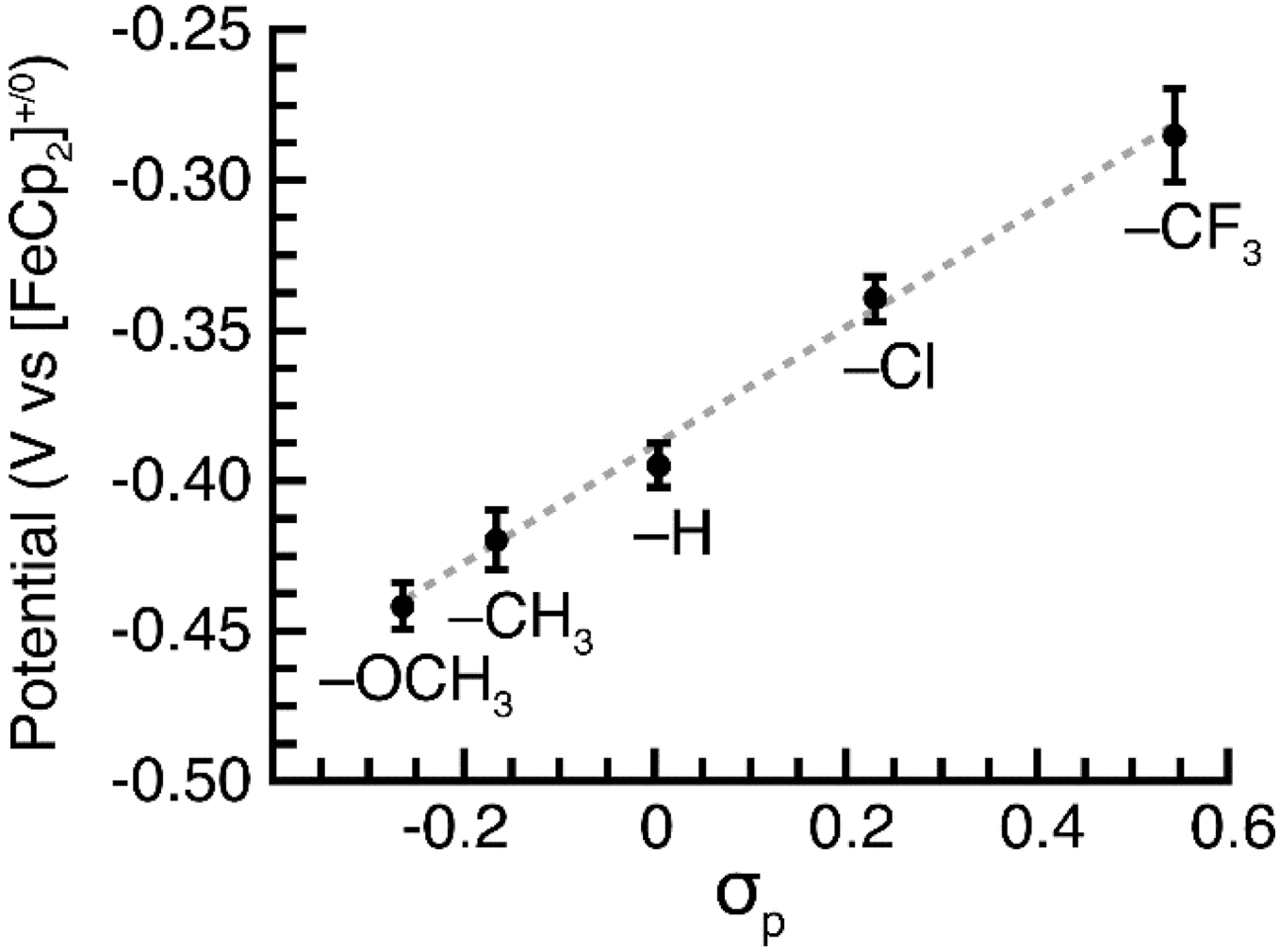

Fig. 4.
Plot of the $E_{1/2}$ of the $Fe^{II/Fe^{III}}$ couple vs. σ_p of the ligand *para*-substituents, with the *para*-substituent R group specified.

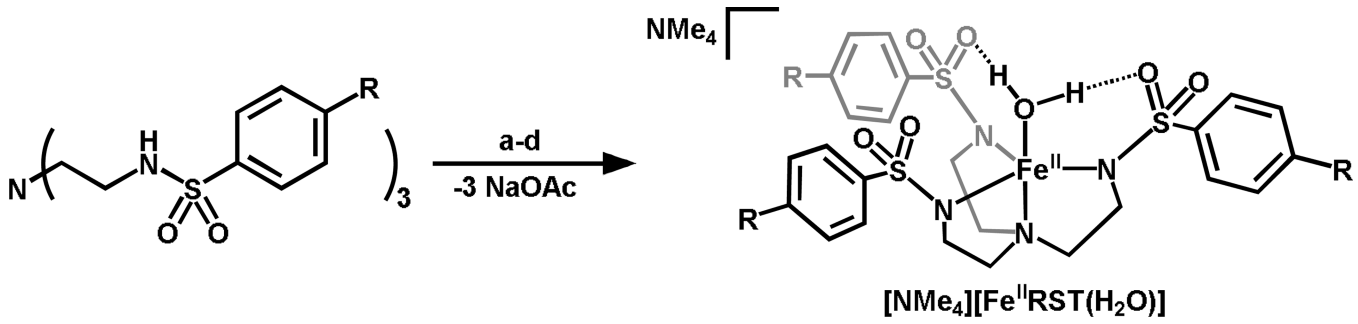

Scheme 1.

Preparation of $[NMe_4][Fe^{II}RST(OH_2)]$ complexes. Conditions: (a) 3 NaH, DMA, N2, rt; (b) $Fe(OAc)_2$, DMA, N_2, rt; (c) NMe_4OAc, DMA, N_2, rt; (d) 4 H_2O, CH_2Cl_2, N_2, rt. R = $–CF_3$, –Cl, –H, $–CH_3$, $–OCH_3$.

Table 1

Selected metrical parameters for the $[Fe^{II}RST(OH_2)]^-$ complexes.

$[Fe^{II}RST(OH_2)]^-$	R =				
Bond distances (Å)	$-CF_3$*	–Cl	–H	$-CH_3$	$-OCH_3$*
Fe1–O1	2.120(3)	2.096(2)	2.139(1)	2.099(2)	2.164(4)
Fe1–N1	2.208(3)	2.219(2)	2.214(1)	2.227(2)	2.226(4)
Fe1–N2	2.010(3)	2.112(2)	2.107(1)	2.086(2)	2.071(4)
Fe1–N3	2.071(3)	2.094(2)	2.098(1)	2.108(2)	2.091(4)
Fe1–N4	2.082(3)	2.070(2)	2.065(1)	2.069(2)	2.041(4)
O1···O2	2.672(3)	2.708(2)	2.697(1)	2.763(2)	2.673(4)
O1···O4	2.782(3)	2.773(2)	2.676(1)	2.701(2)	2.707(4)
O1···O6	3.005(3)	3.087(2)	3.089(1)	3.090(2)	3.089(4)
Average $Fe–N_{eq}$	2.084(3)	2.092(2)	2.090(1)	2.088(2)	2.068(4)
Bond angle (°)					
N1-Fe1-O1	174.91(1)	169.74 (6)	170.91(5)	170.25(7)	173.19(1)
N1-Fe1-N2	80.25(1)	80.11 (6)	79.08(5)	79.17(7)	80.50(1)
N1-Fe1-N3	79.75(1)	78.93 (6)	80.76(5)	80.20(7)	79.63(1)
N1-Fe1-N4	80.98(1)	80.13(6)	80.58(5)	79.85(7)	80.85(1)
N2-Fe1-N3	115.48(1)	115.57(7)	114.60(5)	115.98(7)	112.21(2)
N2-Fe1-N4	120.95(1)	120.18(7)	116.96(5)	115.70(7)	116.40(2)
N3-Fe1-N4	115.24(1)	114.93(7)	119.85(5)	119.02(8)	123.04(2)
τ value	0.859	0.826	0.851	0.854	0.836

*Indicates average values, because of two crystallographically distinct but chemically equivalent complexes in the asymmetric unit cell of these structures.

Polyhedron. Author manuscript; available in PMC 2016 January 08.